Biomaterials and Biomechanics in Bioengineering, *Vol. 3, No. 3 (2016) 129-140*
DOI: http://dx.doi.org/10.12989/bme.2016.3.3.129

Polymeric nanoparticles as dual-imaging probes for cancer management

Jyothi U. Menon[1,2], Parth Jadeja[1,2], Pranjali Tambe[1,2], Dheeraj Thakore[1,2], Shanrong Zhang[3], Masaya Takahashi[3], Zhiwei Xie[4], Jian Yang**[4] and Kytai T. Nguyen[1,2*]

[1]*Bioengineering Department, The University of Texas at Arlington, Arlington, TX, USA 76019*
[2]*Graduate Biomedical Engineering Program, UT Southwestern Medical Center, Dallas, TX, USA 75390*
[3]*Advanced Imaging Research Center, UT Southwestern Medical Center, Dallas, TX, USA 75390*
[4]*Department of Biomedical Engineering, Pennsylvania State University, University Park, PA 16802*

(Received June 29, 2015, Revised September 12, 2016, Accepted Accepted December 16, 2016)

Abstract. This article reports the development of biodegradable photoluminescent polymer (BPLP)-based nanoparticles (NPs) incorporating either magnetic nanoparticles (BPLP-MNPs) or gadopentate dimeglumine (BPLP-Gd NPs), for cancer diagnosis and treatment. The aim of the study is to compare these nanoparticles in terms of their surface properties, fluorescence intensities, MR imaging capabilities, and *in vitro* characteristics to choose the most promising dual-imaging nanoprobe. Results indicate that BPLP-MNPs and BPLP-Gd NPs had a size of 195±43 nm and 161±55 nm, respectively and showed good stability in DI water and 10% serum for 5 days. BPLP-Gd NPs showed similar fluorescence as the original BPLP materials under UV light, whereas BPLP-MNPs showed comparatively less fluorescence. VSM and MRI confirmed that the NPs retained their magnetic properties following encapsulation within BPLP. Further, *in vitro* studies using HPV-7 immortalized prostate epithelial cells and human dermal fibroblasts (HDFs) showed > 70% cell viability up to 100 µg/ml NP concentration. Dose-dependent uptake of both types of NPs by PC3 and LNCaP prostate cancer cells was also observed. Thus, our results indicate that BPLP-Gd NPs would be more appropriate for use as a dual-imaging probe as the contrast agent does not mask the fluorescence of the polymer. Future studies would involve *in vivo* imaging following administration of BPLP-Gd NPs for biomedical applications including cancer detection.

Keywords: nanoparticles; fluorescent; MRI; contrast agent; dual imaging

1. Introduction

Cancer imaging is an important aspect of cancer diagnosis as it can be used for relatively accurate and early detection of the tumor masses in the body, preferably before the start of metastasis (Frangioni 2008). Various imaging modalities have been employed in monitoring the effects of different therapeutic agents on tumor growth (Balu-Maestro *et al.* 2002). Commonly

*Corresponding author, Ph.D., E-mail: knguyen@uta.edu
**Corresponding author, Ph.D., E-mail: jxy30@psu.edu

http://www.techno-press.org/?journal=bme&subpage=8 ISSN: 2465-9835 (Print), 2465-9959 (Online)

used modalities in cancer imaging include positron emission tomography (PET), computed tomography (CT), magnetic resonance imaging (MRI), and single-photon emission computed tomography (SPECT) (Frangioni 2008). However, the use of a single imaging modality sometimes provides insufficient information on the region of interest. For example, although MRI provides three-dimensional information of the region with high spatial resolution, it is limited by its reduced sensitivity to contrast agents. This can affect the information it provides on cellular and molecular processes (Menon *et al.* 2012, Nam *et al.* 2010). On the other hand, PET is extremely sensitive to tracers but has poor resolution (Jennings and Long, 2009). Optical imaging is another modality that is more sensitive than MRI and can provide more accurate information on cellular events; however, it is limited by low spatial resolution and limited tissue penetration depth, which can be only a few millimeters. MRI, on the other hand, has the advantage of deep tissue penetrability (Jennings and Long 2009, Ke *et al.* 2010). Recent developments in the imaging field have demonstrated that the combined use of multiple imaging modalities that complement each other would help in providing a more accurate representation of the disease; thus, aiding in accurate diagnosis and subsequent effective therapy (Townsend 2008). This accurate representation of the disease is because one modality can overcome the limitations of the other; thus, providing a better and more complete picture of the disease following imaging.

In recent times, nanomedicine and imaging have been combined to develop nanoprobes that can be used for multimodal imaging and therapy following delivery. These probes can be used to target the diseased cells so that valuable information about the malignancy can be obtained. These biocompatible nanoprobes can also be used for early-stage diagnosis of cancer and real-time monitoring of tumor growth/shrinkage following release of the therapeutic agents encapsulated within the probes. For example, Nam et al. (Nam *et al.* 2010) developed glycol chitosan nanoparticles containing near-infrared fluorescent (NIRF) dye Cy5.5 for optical imaging and Gd (III) for MR imaging. *In vivo* studies on pectoral subcutaneous murine squamous carcinoma (SCC7) bearing mice showed good accumulation of the particles at the tumor site, which was detected with high accuracy using NIRF imaging and MRI. Similarly, Ke et al. (Ke *et al.* 2010) developed poly (acrylic acid)-iron oxide complexes surface modified with Rhodamine 123 dye for simultaneous MRI and fluorescence imaging. Further, folic acid was conjugated onto the surfaces of these dual-imaging nanoparticles for tumor targeting of KB cells. These nanoprobes showed good internalization within folate receptor-expressing cancer cells and retained their magnetic and fluorescence properties for dual modality imaging. However incorporation of multiple imaging agents could result in larger nanoparticle sizes causing faster clearance from the body, in addition to photobleaching and toxicity issues from the imaging agents used.

Herein, we have developed a dual-imaging enabled nanoparticle system using biodegradable photoluminiscent polymers (BPLP) and either iron oxide (BPLP-MNPs) or Magnevist/ gadopentate dimeglumine (BPLP-Gd) as MRI contrast agents. BPLP-based nanoparticles have already been developed and thoroughly evaluated by our group as biodegradable and biocompatible nanocarriers that can be visualized using optical imaging due to their innate fluorescence (Wadajkar *et al.* 2012, Yang *et al.* 2009). BPLPs are fully degradable polymers with intrinsic fluorescence; thus, they can overcome the limitations of conventional fluorescent agents such as quantum dots and fluorescent dyes. Quantum dots tend to be insoluble in water, cause toxicity, and have relatively weak polarization of the emitted photons (Drbohlavova *et al.* 2009). Fluorescent dyes, on the other hand, have the disadvantage of having low chemical and photo-stability and could undergo photobleaching (Wadajkar *et al.* 2012, Waggoner 2006). In contrast, BPLP is biodegradable, has inherent fluorescence, and can be dispersed in water; thus, overcoming

most of the limitations listed above (Wadajkar *et al.* 2012). Iron oxide nanoparticles have also been extensively evaluated for drug delivery as they exhibit a superparamagnetic property which is useful for MRI, magnetic targeting, and magnetic separation. Further, these particles can be used to generate hyperthermia in the presence of an alternating external magnetic field (Laurent *et al.* 2011, Wadajkar *et al.* 2012). Magnevist or gadopentate dimeglumine is an FDA-approved commercially available gadolinium (Gd)-based compound that can be incorporated in nanoparticles as a contrast agent for MRI. Gadolinium-based contrast agents are considered to be relatively safe, as they do not cause nephrotoxicity like some iodinated x-ray agents. Gadopentate dimeglumine can also undergo hepatobiliary and renal clearance, and hence be cleared easily from the body (Runge 2000). While gadolinium is used as a 'postive' contrast agent, SPIO is usually used as a 'negative' contrast agent (Faucher *et al.* 2011). The objective of this project was to develop biodegradable, dual imaging enabled NPs encapsulating only one imaging agent, which can be used for sustained, controlled drug delivery later if needed. Traditionally, multi-imaging nanoprobes require the incorporation of multiple imaging components. However, this use of multiple imaging agents as seen in literature may result in the formation of particles with large sizes, which may be rapidly cleared from circulation. Our nanoparticle system can circumvent this disadvantage as the intrinsic fluorescence of the polymer used can aid in imaging. This research also focuses on comparing particles containing either iron oxide or gadolinium to choose the most optimal formulation for dual-imaging applications.

2. Materials and methods

2.1 Materials used

Materials used include iron oxide nanoparticles (MNPs) (Meliorum Technologies, Rochester, NY) and Gadopentate Dimeglumine (Magnevist, Jefferson Medical & Imaging, Inc., Oak Ridge, NJ). Adult Human Dermal Fibroblasts (HDFs) were obtained from Invitrogen (Grand Island, NY), while LNCaP and PC3 prostate cancer cell lines were purchased from American Type Culture Collection (ATCC, Manassas, VA). Dulbecco's Modified Eagle's Medium (DMEM), RPMI-1640 medium, penicillin-streptomycin, and trypsin-Ethylenediaminetetraacetic acid (Trypsin-EDTA) were also purchased from Invitrogen Corporation (Grand Island, NY). PrEBM media supplemented with prostate epithelial growth medium (PrEGM) SingleQuot kit was obtained from Clonetics, Lonza (Allendale, NJ). Fetal bovine serum (FBS) was obtained from Atlanta Biological (Lawerenceville, GA). All other materials, if not specified, were purchased from Sigma Aldrich (St. Louis, MO) and used without further purification.

2.2 Polymer synthesis

BPLP-cysteine was synthesized based on the protocol previously described by our group (Yang *et al.* 2009). Briefly, citric acid, 1,8-octanediol and L-cysteine were combined and stirred at 160^{o}C for 20 minutes. Then the temperature was decreased to 140˚C and the contents stirred for 75 minutes. The resulting polymer was dissolved by using 1,4-dioxane, precipitated in DI water, and followed by lyophilization to obtain purified BPLP.

2.3 Synthesis of BPLP-MNPs and BPLP-Gd NPs

BPLP-MNPs were prepared by a standard double emulsion method. To form the first water phase, 10 mg of MNPs was added to deionized (DI) water and dispersed by sonication. 8% w/v BPLP solution in 1,4-dioxane (oil phase) was prepared and the MNP suspension was added to it dropwise. This water-in-oil solution was then sonicated for 5 minutes at 20 W. Following this, it was added dropwise to the second water phase consisting of 400 mg of sodium dodecyl sulfate (SDS) in DI water. The formed emulsion was sonicated further at 50 W for 10 minutes, after which it was stirred overnight to allow solvent evaporation. The particles were collected using an external magnet and lyophilization.

BPLP-Gd NPs were also prepared using a similar procedure as the one described above. The only deviation was the use of Magnevist solution (10 mg of gadopentate dimeglumine in DI water) as the first water phase instead of the MNP solution used in the BPLP-MNPs protocol.

2.4 Nanoparticle characterization

The hydrodynamic diameter, polydispersity index (PDI), and surface charge for both particles were studied using Dynamic Light Scattering (DLS) instrument (Brookhaven Instruments, Holtsville, NY). Electron Microscopy (TEM, FEI Tecnai G2 Spirit BioTWIN, Hillsboro, OR) was used to visualize particle morphology. In addition to physical properties, the chemical characterization of BPLP-MNPs and BPLP-Gd NPs was carried out using Fourier Transform Infra-Red (FTIR) spectroscopy (Nicolet-6700, Thermo Fisher Scientific, Waltham, MA). The stability of these particles in media containing 10% serum and DI water at 37^{o}C was also examined. For this study, the particles were dispersed in the designated solution and incubated at 37^{o}C. Particle size was measured using DLS every 24 hours for 5 days. Further, the fluorescence emitted by the particles was quantified using a plate reader (Infinite M200, Tecan, Durham, NC). 1 mg/ml suspensions of BPLP-Gd NPs, BPLP-MNPs, and BPLP were prepared in DI water and added to a 96 black well-plate. Fluorescence intensities were taken at λ_{ex} 370 nm and λ_{em} 440 nm.

Finally, the magnetic properties of both particles were characterized using a vibrating sample magnetometry (VSM). Briefly, the lyophilized sample was dispersed in epoxy gel and applied to a holder which was then inserted into the VSM (EV7, KLA-Tencor, Milpitas, CA). The particles were also dispersed in 0.5% w/v agarose phantoms at pre-determined concentrations (0.25, 0.5, 1, and 2 mg/ml) and visualized using MRI. Agarose only and BPLP only were used as controls. Imaging was done on a 7T Agilent (Varian) MRI Scanner which had a built in fsems sequence. The parameters used include TR=2500 ms; TE=10 ms (for BPLP-MNPs) or 60 ms (for BPLP-Gd NPs); matrix=256×256; field of view of 40mm×40mm; slice thickness=1 mm.

2.5 In vitro studies

2.5.1 Cell viability studies

Studies were conducted to evaluate the viability of immortalized prostate epithelial cells (PZ-HPV-7) and human dermal fibroblasts (HDFs) on exposure to BPLP-MNPs and BPLP-Gd NPs. First, the cells were plated at a density of 5000 cells/well in a 96 well plate and incubated at 37^{o}C and 5% CO_2 for a day to allow cell attachment. Then the media in each well was replaced with NP suspensions at pre-determined concentrations [0 (control), 10, 20, 40, 80, 100, 250, and 500 μg/ml] followed by incubation for 24 hours. The cell viability was then determined using colorimetric

MTS assays (Cell Titer 96® Aqueous One Solution Cell Proliferation Assay, Promega, Madison, WI) via manufacturer's instructions and plotted as a percentage of viable cells per the control group.

2.5.2 Cellular uptake

PC3 and LNCaP prostate cancer cells were seeded at 5000 cells/well seeding density in a 96 well plate and incubated at 37^{o}C and 5% CO_2 to facilitate cell attachment. The following day, NP suspensions at varying concentrations (0, 50, 100, 250, and 500 μg/ml) were added to each well, and the cells were incubated at 37^{o}C for 2 hours. The cells were then washed thrice with PBS, and 1% Triton X-100 was added to all the wells for cell lysis. This cell lysate was used to quantify the total amount of particles taken up by the cells and normalized against the amount of cell protein per well. In the case of cells incubated with BPLP-Gd NPs, the particles were quantified using fluorescence emitted and correlated with a NP standard curve. In the case of BPLP-MNPs, it was observed that iron oxide blocks the fluorescence emitted by the contents in each well. Therefore, these NPs were quantified using a standard iron assay correlated with a NP standard curve. In the case of BPLP-MNPs as well as BPLP Gd NPs, cell protein was quantified using BCA protein assays (Pierce, Fisher Scientific, Hampton, NH).

2.6 Statistical analysis

Experiments were conducted in quadruplicates. Statistical evaluation of data obtained was done by two-way analysis of variance (ANOVA) using StatView (V 5.0.1, SAS Institute Inc., Cary,NC). Data was considered to be statistically significant when $p<0.05$ and using post hoc comparisons

3. Results and discussion

This work discusses the development and physical-chemical characterization of NPs with dual imaging capabilities, using BPLP encapsulated with either SPIO or Gd (Magnevist). We have previously demonstrated the applicability of BPLP towards the synthesis of fluorescent NPs (Wadajkar *et al.* 2012). These NPs can overcome limitations of commonly used fluorescent probes like quantum dots and dyes, such as photobleaching and toxicity (Wadajkar *et al.* 2012, Waggoner 2006). In order to determine the biodistribution of NPs within the body, it is advisable to incorporate components that can be imaged using different modalities within the same particle. Therefore the BPLP NPs developed in this work were made to incorporate either iron oxide or Gd, so that the resultant NPs can be visualized by both optical imaging and MRI.

3.1 Physical, chemical and magnetic properties

Particle size measurements using the DLS detector indicated that BPLP-Gd NPs and BPLP-MNPs had hydrodynamic diameters of 161 ± 55 nm and 195 ± 43 nm, respectively. Thus, these particles would be appropriate for systemic delivery since previous studies have shown that particles >500 nm tend to be taken up rapidly by the reticuloendothelial system and subsequently eliminated from the body (Cho *et al*. 2012, Liao *et al.* 2012). A surface charge of -23.3 mV and -30.7 mV for BPLP-MNP's and BPLP-Gd NPs, respectively indicates that the particles are stable. High zeta potential values of nanoparticles have indicated that the electrostatic repulsion between the

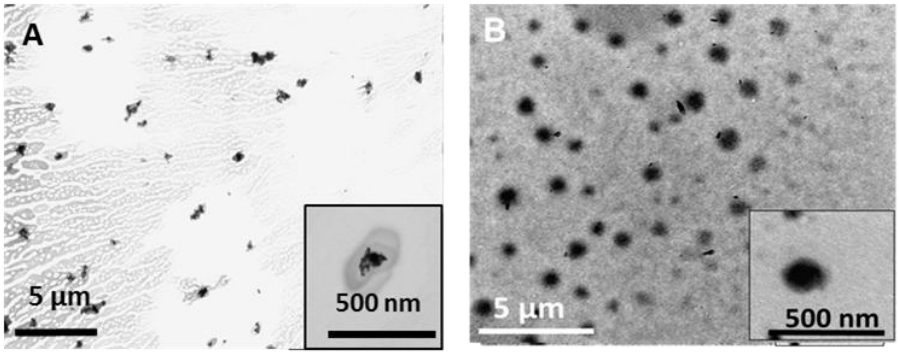

C

NP	Diameter (nm)	Polydispersity	Zeta Potential (mV)
BPLP-MNPs	195 ± 43	0.29	-23.3
BPLP-Gd NPs	161 ± 55	0.16	-30.7

Fig. 1 Physical characterization of BPLP-MNPs and BPLP-Gd NPs. TEM images indicating the morphology of (A) BPLP-MNPs and (B) BPLP-Gd NPs. (C) Analysis of DLS data indicate that the average hydrodynamic diameters of both particles were <200 nm. The negative zeta potential is indicative of the good stability of the particles.

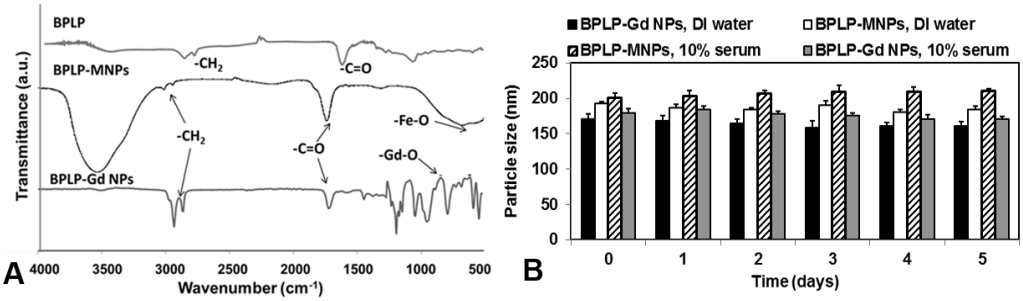

Fig. 2 FTIR and stability studies of BPLP-MNPs and BPLP-Gd NPs. (A) FTIR spectra of BPLP NPs, BPLP-Gd NPs, and BPLP-MNPs confirming the successful incorporation of all components in the respective nanoparticle systems. (B) Stability studies in DI water and serum at 37oC demonstrate that both particles were relatively stable in both solutions at physiological temperature with no significant particle aggregation, which is corresponding to an increase in the particle size, up to 5 days.

particles dominates the van der Waals forces of attraction; thus, stabilizing the particles in solution (Freitas and Muller 1998, Liu and Luijten 2004).

Further, TEM images indicate that the particles are relatively spherical with the BPLP-MNPs having a dark core due to the presence of iron oxide (Fig. 1). The chemical composition of BPLP alone, BPLP-Gd NPs, and BPLP-MNPs was confirmed using FTIR as shown in Fig. 2A. The–CH_2 group present in the polymer backbone gave a peak at around 2980 cm^{-1} for all three tested samples. Further, the peaks at 1550 cm^{-1} and 1721 cm^{-1} represent the (-C=O) group for citric acid and –C(=O)NH group for cysteine, respectively. The presence of iron oxide in BPLP-MNPs is confirmed by the peak at 520 cm^{-1}, whereas the presence of Gd-O is confirmed by the peaks from 500 to 1000 cm^{-1}.

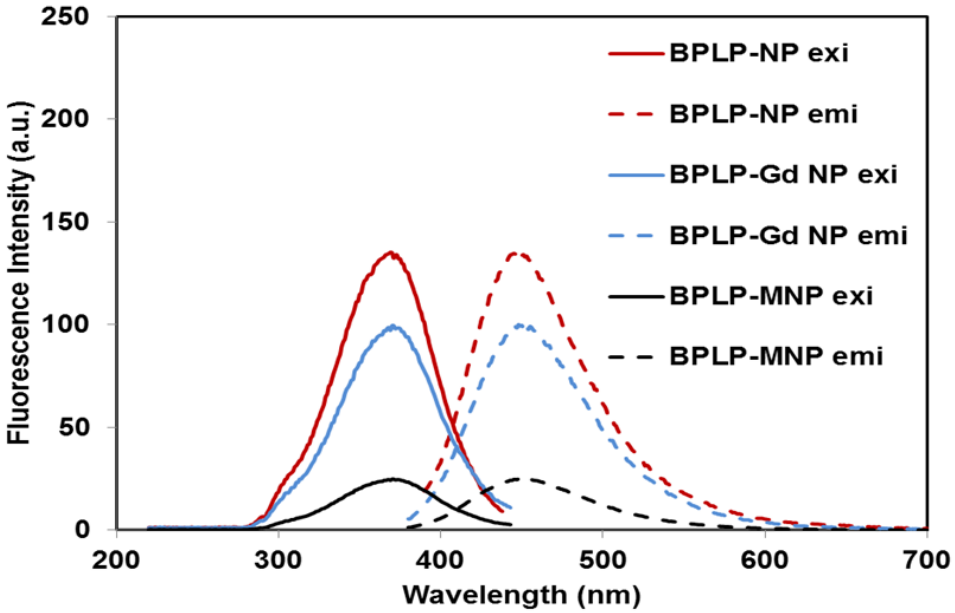

Fig. 3 Fluorescence spectra of BPLP-MNPs and BPLP-Gd NPs. Fluorescence scans of BPLP NPs, BPLP-MNPs, and BPLP-Gd NPs demonstrating that both BPLP NPs and BPLP-Gd NPs had similar excitation and emission peaks, while BPLP-MNPs showed much weaker fluorescence at the same wavelengths

Results from the stability study indicate that both types of particles maintained their hydrodynamic diameters consistently over a period of 5 days, indicating that they are stable and do not aggregate in solutions such as serum and DI water at a physiological temperature (Fig. 2B). These results concur with the high zeta potential values observed by us for these particles, which was also an indicator of good stability. MNP-containing BPLP NPs previously developed by our lab also showed a similar stability profile up to 9 days in the culture medium (Wadajkar *et al.* 2012).

3.2 Optical imaging properties

Fluorescence excitation and emission spectra of both particles was taken to confirm their fluorescence imaging capabilities (Fig. 3). It was observed that the excitation and emission spectra (λ_{ex} = 365 nm , λ_{em} = 445 nm) of BPLP-Gd NPs showed a similar pattern as BPLP NPs with minimal loss in fluorescence intensity. On the other hand, BPLP-MNPs showed a significant decrease in fluorescence intensity compared to BPLP NPs. Gd did not significantly reduce the fluorescence emission from the BPLP. MNPs and Gd alone did not give any fluorescence (data not shown).

Our results are in concurrence with previous studies by Jarzyna et al. (Jarzyna *et al.* 2009), where incorporation of a lipophilic NIR dye and iron oxide in soybean oil core nanoemulsion resulted in highly reduced emission intensity from the dye. Incorporation of iron oxide and quantum dots within oil droplets have also reportedly resulted in reduced fluorescence intensity of the quantum dots due to the presence of the iron oxide (Mandal *et al.* 2005, Wadajkar *et al.* 2012).

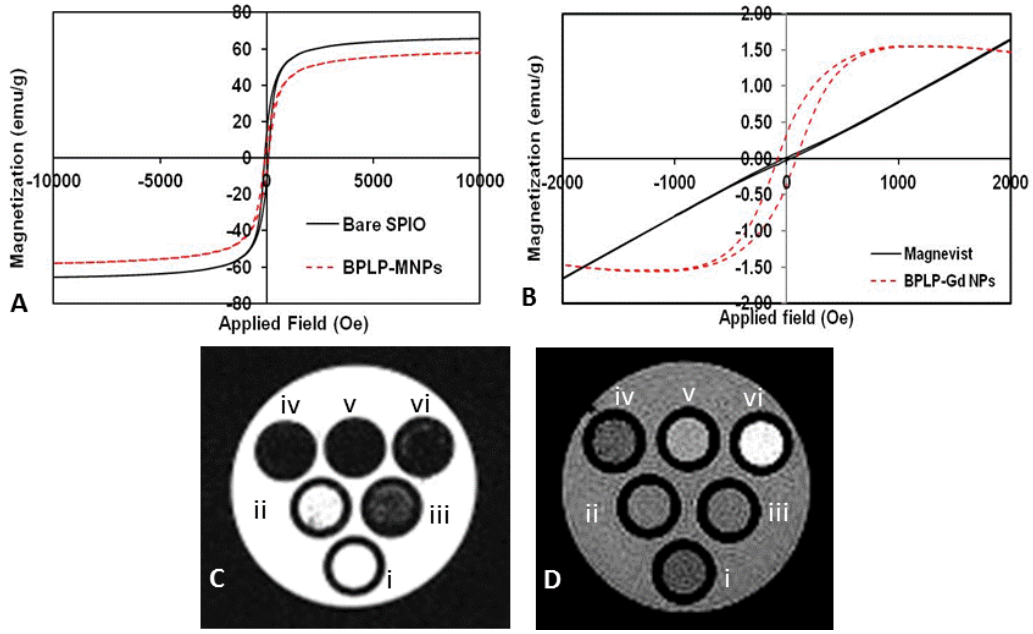

Fig. 4 Magnetic properties of NPs. Hysteresis loops of (A) BPLP-MNPs obtained using VSM shows that the particles had similar hysteresis pattern as bare SPIO. (B) BPLP-Gd NPs also showed a hysteresis loop while bare Gd showed a proportional relationship between the applied magnetic field and magnetization. MRI images of agarose phantoms containing (C) BPLP-MNPs and (D) BPLP-Gd NPs [(i) Agarose only, (ii) BPLP NPs only, (iii) 0.25 mg/ml NPs, (iv) 0.5 mg/ml NPs, (v) 1 mg/ml NPs, (vi) 2 mg/ml NPs] indicating increasing negative contrast with increasing BPLP-MNPs concentrations and greater contrast with increasing BPLP-Gd NPs concentrations

This occurs due to the absorption of light by the iron oxide nanoparticles, thereby reducing the fluorescence emission from the fluorescent components. Confining the MNPs to the core of the NPs by coating them with substances such as oleic acid may help in improving the fluorescence of the final NP system (Mandal *et al.* 2005).

3.3 MR Imaging properties

After studying the fluorescence properties, the particles were further analyzed in terms of their magnetic properties and MR imaging capabilities. Results obtained using VSM demonstrated that BPLP-MNPs have a similar hysteresis loop as bare MNPs, indicating that the MNPs did not lose their magnetic characteristics following encapsulation within BPLP (Fig. 4A). However, the saturation magnetization of BPLP-MNPs was 58 emu/g compared to bare MNPs which had a saturation magnetization of 66 emu/g. This could have occurred because the diamagnetic polymer coating caused a decrease in the magnetic dipolar interaction (Sahoo *et al.* 2013). A remnence of 6.2 $M_rM_s^{-1}$ and coercivity of 58.27 Oe was observed for BPLP-MNPs as opposed to the 7.4 $M_rM_s^{-1}$ remanence and 62.5 Oe coercivity observed in bare MNPs. In the case of bare Gd, a relatively straight line was observed using VSM (Fig. 4B) indicating that it is paramagnetic in nature, similar to what has been observed in previous studies (Bridot *et al.* 2007, Das *et al.* 2010, Gossuin *et al.* 2008). This means that there will be no saturation of magnetic moment for Gd with an increase in

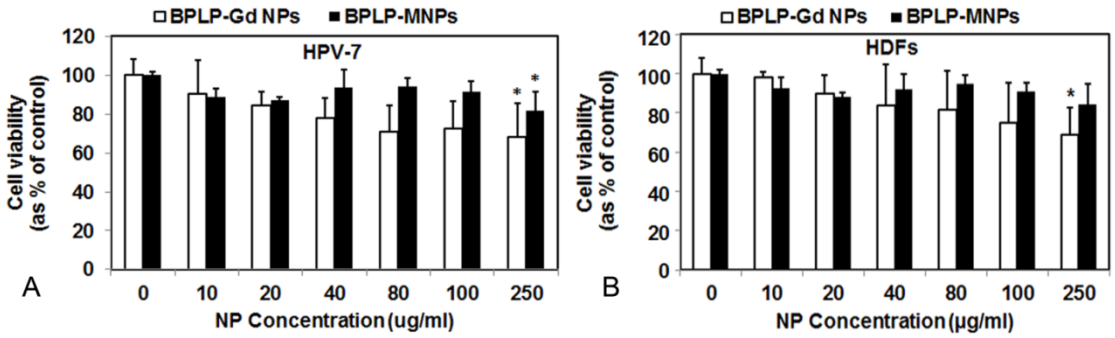

Fig. 5 *In vitro* cytocompatibility of BPLP-MNPs and BPLP-Gd NPs. Cell viability on treatment with varying concentrations of BPLP-MNPs and BPLP-Gd NPs for 24 hours. They were quantified using MTS assays. (A) HDFs and (B) HPV-7 cells showed good cytocompatibility up to 100 µg/ml on treatment with both particles (no significance with the control group). About >70% of the cells was viable at 250 µg/ml NP concentration compared to that of the 0 µg/ml group (Control) (*p<0.05 w.r.t cell viability at 0 µg/ml, n=4)

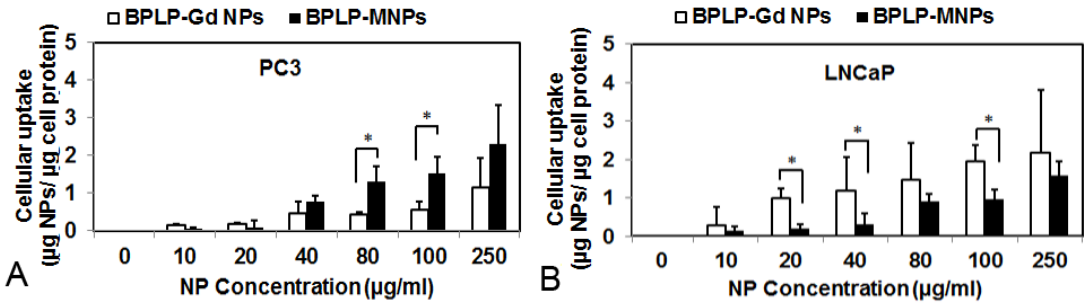

Fig. 6 Cellular uptake of BPLP-MNPs and BPLP-Gd NPs by prostate cancer cells. *In vitro* cellular uptake studies on treatment with varying concentrations of BPLP-MNPs and BPLP-Gd NPs for 2 hours, quantified using fluorescence measurements (BPLP-Gd NP quantification), iron assays (BPLP-MNPs quantification), and BCA assay (cell protein quantification) (A) PC3 and (B) LNCaP prostate cancer cells. The results indicate that the particles were taken up by both cell lines in a dose-dependent manner. Significantly higher uptake of BPLP-MNPs was seen by PC3 cells while significantly higher BPLP-Gd NPs uptake occurred in LNCaP cells (*p<0.05, n=4).

the applied magnetic field. However, in the case of BPLP-Gd NPs, a slight hysteresis was observed following coating with polymer indicating that the nanoparticles exhibited slightly superparamagnetic characteristics. This is similar to the superparagmagnetic behavior observed by Azizian et al. (Azizian *et al.* 2012) when coating Gd oxide with diethylene glycol. MRI studies of agarose phantoms consisting of these nanoparticles were further performed to investigate if they could be used for visualization via MRI. A significantly dark negative contrast was observed in the BPLP-MNPs samples with increasing NP concentration (Fig. 4C). This negative contrast could be observed even at a low NP concentration of 0.25 mg/ml. The signal intensity was found to drop by 83%, 90%, 95%, and 97% for 0.25mg/ml, 0.5 mg/ml, 1 mg/ml, and 2 mg/ml concentrations, respectively (compared to the signal intensity of the control [agarose only]). In the case of agarose phantoms containing Gd, an enhancement in the MR signals was observed with increasing concentration of BPLP-Gd NPs (Fig. 4D). The increase in signals was found to be 113%, 116%,

134%, and 179%, respectively for 0.25mg/ml, 0.5 mg/ml, 1 mg/ml, and 2 mg/ml BPLP-Gd NPs concentrations (compared to the signal intensity of the control [agarose only]). The decrease in signal intensity observed with increasing BPLP-MNPs concentration and the enhanced MR signals with increasing BPLP-Gd NPs concentration are in agreement with previous studies done by our group as well as others on NPs encapsulating these contrast agents (Cho *et al.* 2012, Liao *et al.* 2012, Wadajkar *et al*. 2012, Wadajkar *et al*. 2013).

3.4 In vitro cytocompatiility studies

Our cytotoxicity results demonstrate that both BPLP-Gd NPs and BPLP-MNPs were cytocompatible with HPV-7 cells and HDFs. More than 70% of the cells compared to the control group (cells in media only, 0 μg/ml) were viable at 250 μg/ml concentration for both particles (Figs. 5A, B). For both cell lines BPLP-MNPs showed a slightly higher cytocompatibility than BPLP-Gd NPs although this difference in cytocompatibility was not significant. BPLP-based films prepared by our group have previously shown good cytocompatibility with 3T3 mouse fibroblasts *in vitro* (Yang *et al.* 2009). The BPLP-based scaffolds also did not trigger major inflammatory responses *in vivo* for up to 5 months (Yang *et al.* 2009). Our BPLP-MNP cytocompatibility was in the same range as that observed for BPLP-MNPs synthesized previously by us, which also showed good cytocompatibility with HDFs up to 500 μg/ml concentration (Wadajkar *et al.* 2012). These results show that the BPLP-MNPs and BPLP-Gd NPs are cytocompatible and can be administered up to a dose of 250 μg/ml for imaging and drug delivery applications.

3.5 In vitro cellular uptake studies

A cellular uptake study was conducted to determine the optimal concentration of BPLP-Gd NPs and BPLP-MNPs at which saturation of uptake occurs in PC3 and LNCaP prostate cancer cells. A dose-dependent increase in uptake of the particles was observed in the case of both cancer cells (Figs. 6A, B). BPLP-MNPs were taken up at a significantly larger amount by PC3 cells than LNCaP cells, while BPLP-Gd NPs were taken up in greater amounts by LNCaP cells. It has been reported previously that treatment of PC3 cells with Gd-based products caused disruption of zinc metabolism resulting in increased intracellular free zinc levels (Magda *et al.* 2005). Zinc is known to play a key role in regulating biological pathways related to carcinogenesis and elevated zinc levels can have cytotoxic effects on the cells. This disruption in cell metabolism could possibly have affected the uptake of Gd by PC3 cells. Further, Gd has also been shown to possibly inhibit phosphorylation of extracellular-signal-regulated kinase (ERK) and mitogen-activated protein kinase (p38 MAPK) signaling pathways resulting in inhibition of PC3 cell migration and colony forming ability, leading eventually to apoptotic death (Wang *et al.* 2011). These results were not observed by the same authors in the same work with DU145 prostate cancer cells, although the reason for this differential response to Gd remains unclear. LNCaP, on the other hand, is a non-migratory cell line (Maroto *et al.* 2012) and may have been affected to a lesser extent by Gd uptake than the PC3 cells.

5. Conclusions

In summary, two different types of NPs for dual-imaging were synthesized. The BPLP-MNPs

and BPLP-Gd NPs showed sizes less than 200 nm, which are optimal for avoiding clearance by RES, and showed good magnetic and MR imaging capabilities. While BPLP-Gd NPs showed comparable fluorescence as that of BPLP NPs, the MNPs within BPLP-MNPs significantly quenched the fluorescence of the polymer. Both NPs showed good cytocompatibility with fibroblasts and normal prostate epithelial cells up to 100 μg/ml concentration. While BPLP-MNPs were taken up more in PC3 cells, BPLP-Gd NPs were taken up in more quantities by LNCaP cells. Our results indicate that BPLP-Gd NPs may be more appropriate in maintaining the dual imaging capabilities of its components. However, steps must be taken to improve the magnetic susceptibility of Gd for MRI applications. Future studies will involve encapsulation of therapeutic agents and studying their release kinetics. *In vivo* studies will also be conducted to confirm the *in vivo* theranostic capabilities of these multi-functional dual-imaging capable NPs.

Acknowledgements

The authors would like to acknowledge funding support from the National Institutes of Health (NIH) U01 HL111146, R01 HL118498, NIBIB EB012575, and NCI CA182670 grants. We also acknowledge the assistance from Dr. Aniket Wadajkar in obtaining TEM images for BPLP-MNPs.

References

Azizian, G., Riyahi-Alam, N., Haghgoo, S., Moghimi, H.R., Zohdiaghdam, R., Rafiei, B. and Gorji, E. (2012), "Synthesis route and three different core-shell impacts on magnetic characterization of gadolinium oxide-based nanoparticles as new contrast agents for molecular magnetic resonance imaging", *Nanoscale Res., Lett.*, **7**(1), 1-10.

Balu-Maestro, C., Chapellier, C., Bleuse, A., Chanalet, I., Chauvel, C. and Largillier, R. (2002), "Imaging in evaluation of response to neoadjuvant breast cancer treatment benefits of MRI", *Breast Cancer Res. Treat.*, **72**(2), 145-152.

Bridot, J.L., Faure, A.C., Laurent, S., Riviere, C., Billotey, C., Hiba, B., ... and Muller, R. (2007), "Hybrid gadolinium oxide nanoparticles: multimodal contrast agents for in vivo imaging", *J. Am. Chem. Soc.*, **129**(16), 5076-5084.

Cho, H.J., Yoon, H.Y., Koo, H., Ko, S.H., Shim, J.S., Cho, J.H., ... and Kim, D.D. (2012), "Hyaluronic acid-ceramide-based optical/MR dual imaging nanoprobe for cancer diagnosis", *J. Control. Release*, **162**(1), 111-118.

Das, G.K., Heng, B.C., Ng, S.C., White, T., Loo, J.S.C., D'Silva, L., ... and Tan, T.T.Y. (2010), "Gadolinium oxide ultranarrow nanorods as multimodal contrast agents for optical and magnetic resonance imaging", *Langmuir*, **26**(11), 8959-8965.

Drbohlavova, J., Adam, V., Kizek, R. and Hubalek, J. (2009), "Quantum dots-characterization, preparation and usage in biological systems", *Int. J. Molecular Sci.*, **10**(2), 656-673.

Faucher, L., Gossuin, Y., Hocq, A. and Fortin, M.A. (2011), "Impact of agglomeration on the relaxometric properties of paramagnetic ultra-small gadolinium oxide nanoparticles", *Nanotech.*, **22**(29), 295103.

Frangioni, J.V. (2008), "New technologies for human cancer imaging", *J. Clinic. Oncol.*, **26**(24), 4012-4021.

Freitas, C. and Müller, R.H. (1998), "Effect of light and temperature on zeta potential and physical stability in solid lipid nanoparticle (SLN™) dispersions", *Int. J. Pharmaceut.*, **168**(2), 221-229.

Gossuin, Y., Hocq, A., Vuong, Q.L., Disch, S., Hermann, R.P. and Gillis, P. (2008), "Physico-chemical and NMR relaxometric characterization of gadolinium hydroxide and dysprosium oxide nanoparticles", *Nanotech.*, **19**(47), 475102.

Jarzyna, P.A., Skajaa, T., Gianella, A., Cormode, D.P., Samber, D.D., Dickson, S.D., ... and Mulder, W.J.

(2009), "Iron oxide core oil-in-water emulsions as a multifunctional nanoparticle platform for tumor targeting and imaging", *Biomater.*, **30**(36), 6947-6954.

Jennings, L.E. and Long, N.J. (2009), "Two is better than one'-probes for dual-modality molecular imaging", *Chem. Comm.*, (24), 3511-3524.

Ke, J.H., Lin, J.J., Carey, J.R., Chen, J.S., Chen, C.Y. and Wang, L.F. (2010), "A specific tumor-targeting magnetofluorescent nanoprobe for dual-modality molecular imaging", *Biomater.*, **31**(7), 1707-1715.

Laurent, S., Dutz, S., Häfeli, U.O. and Mahmoudi, M. (2011), "Magnetic fluid hyperthermia: focus on superparamagnetic iron oxide nanoparticles", *Adv. Colloid Interface Sci.*, **166**(1), 8-23.

Liao, A.H., Liu, H.L., Su, C.H., Hua, M.Y., Yang, H.W., Weng, Y.T., ... and Yen, T.C. (2012), "Paramagnetic perfluorocarbon-filled albumin-(Gd-DTPA) microbubbles for the induction of focused-ultrasound-induced blood–brain barrier opening and concurrent MR and ultrasound imaging", *Phys. Medicine Biol.*, **57**(9), 2787.

Liu, J. and Luijten, E. (2004), "Stabilization of colloidal suspensions by means of highly charged nanoparticles", *Phys. Rev. Lett.*, **93**(24), 247802.

Magda, D., Lecane, P., Miller, R.A., Lepp, C., Miles, D., Mesfin, M., ... and Karaman, M.W. (2005), "Motexafin gadolinium disrupts zinc metabolism in human cancer cell lines", *Cancer Res.*, **65**(9), 3837-3845.

Mandal, S.K., Lequeux, N., Rotenberg, B., Tramier, M., Fattaccioli, J., Bibette, J. and Dubertret, B. (2005), "Encapsulation of magnetic and fluorescent nanoparticles in emulsion droplets", *Langmuir*, **21**(9), 4175-4179.

Maroto, R., Kurosky, A. and Hamill, O.P. (2012), "Mechanosensitive Ca2+ permeant cation channels in human prostate tumor cells", *Channels*, **6**(4), 290-307.

Menon, J.U., Gulaka, P.K., McKay, M.A., Geethanath, S., Liu, L. and Kodibagkar, V.D. (2012), "Dual-modality, dual-functional nanoprobes for cellular and molecular imaging", *Theranostics*, **2**(12), 1199-1207.

Nam, T., Park, S., Lee, S.Y., Park, K., Choi, K., Song, I.C., ... and Kim, K. (2010), "Tumor targeting chitosan nanoparticles for dual-modality optical/MR cancer imaging", *Bioconjugate Chem.*, **21**(4), 578-582.

Runge, V.M. (2000), "Safety of approved MR contrast media for intravenous injection", *J. Magnetic Resonance Imag.*, **12**(2), 205-213.

Sahoo, B., Devi, K.S.P., Banerjee, R., Maiti, T.K., Pramanik, P. and Dhara, D. (2013), "Thermal and pH responsive polymer-tethered multifunctional magnetic nanoparticles for targeted delivery of anticancer drug", *ACS Appl. Mater. Interf.*, **5**(9), 3884-3893.

Townsend, D.W. (2008), "Dual-modality imaging: combining anatomy and function", *J. Nuclear Medicine*, **49**(6), 938-955.

Wadajkar, A.S., Kadapure, T., Zhang, Y., Cui, W., Nguyen, K.T. and Yang, J. (2012), "Dual-imaging enabled cancer-targeting nanoparticles", *Adv. Healthcare Mater.*, **1**(4), 450-456.

Wadajkar, A.S., Menon, J.U., Tsai, Y.S., Gore, C., Dobin, T., Gandee, L., ... and Hsieh, J.T. (2013), "Prostate cancer-specific thermo-responsive polymer-coated iron oxide nanoparticles", *Biomater.*, **34**(14), 3618-3625.

Waggoner, A. (2006), "Fluorescent labels for proteomics and genomics", *Current Opinion Chem. Biol.*, **10**(1), 62-66.

Wang, P., Zou, X.M., Huang, J., Zhang, T.L. and Wang, K. (2011), "Gadolinium inhibits prostate cancer PC3 cell migration and suppresses osteoclast differentiation *in vitro*", *Cell Biol. Int.*, **35**(11), 1159-1167.

Yang, J., Zhang, Y., Gautam, S., Liu, L., Dey, J., Chen, W., ... and Tang, L. (2009), "Development of aliphatic biodegradable photoluminescent polymers", *Proceedings of the National Academy of Sciences*, **106**(25), 10086-10091.